SUPPORTING INFORMATION APPENDIX (SI Appendix)

Unraveling submicron mechanical heterogeneity by three-dimensional X-ray micro-diffraction

Runguang Li[a,1], Qingge Xie[a,1], Yan-Dong Wang[a,2], Wenjun Liu[b,2], Mingguang Wang[c], Guilin Wu[d], Xiaowu Li[c], Minghe Zhang[a], Zhaoping Lu[a], Chang Geng[c], Ting Zhu[e,2]

[a]State Key Laboratory for Advanced Metals and Materials, University of Science and Technology Beijing, Beijing 100083, China

[b]Advanced Photon Source, Argonne National Laboratory, Argonne, IL 60439, USA

[c]Key Laboratory for Anisotropy and Texture of Materials, School of Materials Science and Engineering, Northeastern University, Shenyang 110004, China

[d]School of Materials Science and Engineering, Chongqing University, Chongqing 400044, China

[e]Woodruff School of Mechanical Engineering, Georgia Institute Technology, Atlanta, GA 30332, USA

[1]Contributed equally to this work.

[2]The correspondence should be addressed to YDW (ydwang@ustb.edu.cn), WL (wjliu@anl.gov) or TZ (ting.zhu@me.gatech.edu).

S1. Material and method for sample preparation

S2. Fatigue testing

S3. Synchrotron based X-ray micro-diffraction (μXRD) measurements

S4. Determination of slip planes of the observed slip bands

S5. Evolution of diffraction profiles near the intersection of slip bands

S6. Analysis of elastic strain field near the intersection of dislocation pile-ups

S7 Dislocation dynamics simulations

S1. Material and method for sample preparation

The AL6XN stainless steel sheet used in this work was purchased from Nippon Yarkin Kogyo CO., LTD. The sheet was produced by hot rolling with a final thickness of 15 mm. The material has a single-phase face-centered-cubic (FCC) structure, with the lattice constant $a = 0.361\,\mathrm{nm}$. The grain sizes range from 80 to 120 μm. The chemical composition of this material is listed in **Table S1**. Samples for mechanical testing were cut from the sheet after 1160 °C solution treatment followed by water quenching. **Fig. S1** shows a representative stress-strain curve under uniaxial tension.

Table S1. Chemical composition of AL6XN austenite stainless steel (wt%)

C	Si	Mn	P	S	Ni	Cr	Mo	Cu	N	Fe
0.016	0.63	0.28	0.022	0.000	23.8	21.7	6.6	0.19	0.21	base

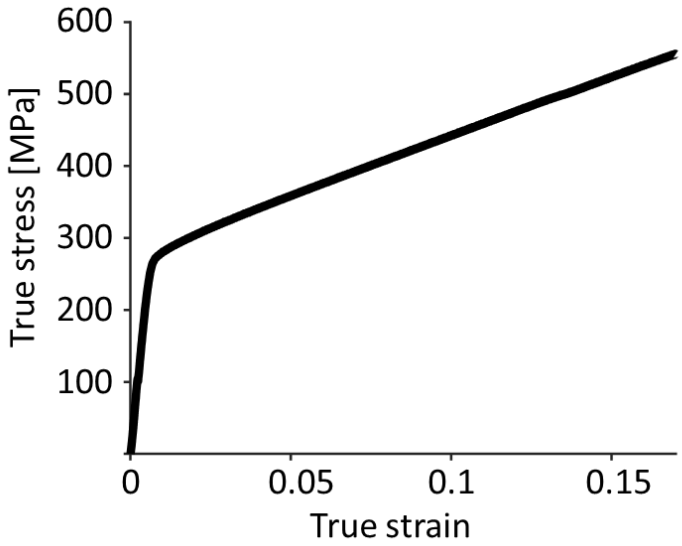

Fig. S1. The true stress versus true strain curve of as-received AL6XN stainless steel.

S2. Fatigue testing

The standard rod-shaped samples were used in fatigue tests. The dimension in the sample gauge section was 8 mm in diameter and 20 mm in length. The fatigue test was conducted under a total strain control on a MTS-810 Servo-hydraulic Universal Testing Machine, with the maximum strain amplitude of 0.3%, the cycle asymmetry coefficient $R = -1$, and

the load frequency of 0.5 Hz. Strain was measured with an extensometer mounted directly on the gauge section. The initial load was tension and the end load was compression. All fatigue tests were carried out at room temperature in air.

S3. Synchrotron based X-ray micro-diffraction (μXRD) measurements

Dog-bone-shaped tensile specimens were cut from a fatigue sample after 29,000 cycles. The tensile loading axis of these specimens is aligned with the fatigue loading direction. Dimensions of the gauge section of the tensile specimen were 2.75 mm (length)×1.25 mm (width)×0.2 mm (thickness). The incident X-ray beam was aligned at 45 °to the tensile loading axis and thus the diffraction vector was nearly along the through-thickness direction, i.e. the normal direction (ND) of side face of the specimen. μXRD measurements were first performed without loading. Then, in-situ μXRD measurements were made after applying a 0.5% engineering tensile strain, so as to investigate the effect of further loading on the fatigued grains.

Specifically, the spatially-resolved 3D μXRD measurements were conducted by using differential-aperture X-ray microscopy (DAXM) at beamline 34-ID-E of the Advanced Photon Source in Argonne National Laboratory. An X-ray microbeam (polychromatic or monochromatic) was focused to about 0.5 μm × 0.5 μm by a pair of elliptical Kirkpatrick–Baez focusing mirrors. **Fig. S2a** is a schematic illustration of the diffraction geometry. Diffracted X-ray beams are recorded on an X-ray area detector. The depth resolution is provided by scanning a 100-μm-diameter platinum wire as diffracted-beam profiler in a knife-edge fashion. By triangulation, the origins of the X-rays can be determined on a pixel-by-pixel basis. A typical scanning step of 1.4 μm gives the depth resolution of ~1.0 μm.

We scanned an area of 200 μm × 80 μm with a step of 1 μm by 1 μm, with the total points of 1,6000 in 3D mode for the sample before loading. We scanned the energy in the step of 2 eV for each pixel. The total area of the 3D+energy mode scanning before and after

loading are 130.5 μm × 91 μm and 109.5 μm × 91 μm with the same step of 1.5 μm by 1 μm, respectively.

In the monochromatic beam mode, the energy is scanned through the Bragg peak in 2 eV steps. By combining data from all of the energies and wire positions, the X-ray intensity at each pixel on the detector was determined as a function of photon energy at each depth step. Since we know the locations of the pixels on the detector relative to the incident beam, the diffraction angle can be calculated and converted to diffraction vector **q** in reciprocal *k*-space. By histogramming all the data of pixels around peak reflection as a function of |**q**|, the diffraction line profile (diffraction intensities vs. |**q**|) can be obtained at each sample depth. **Fig. S2b** shows a |**q**|-distribution of (480) reflection located at a typical 'matrix' region inside a strained crystal. The predicted |**q**| is shown by the dotted vertical line, and the scattering from the reflection is clearly shifted to higher |**q**|.

By scanning sample along transverse direction (TD), an incident X-ray slicing plane at 45 º to the sample surface can be measured, hence maps of crystal orientation (in polychromatic beam mode), diffraction peak profile FWHM and lattice strain (in monochromatic beam mode) are obtained.

We used Lorentz function, i.e. $L(x) = \frac{1}{2\pi}\frac{h\Gamma}{(x-x_0)^2+(\Gamma/2)^2} + b$, to fit the diffraction peak in the energy-scanning mode in order for obtaining the lattice strain and FWHM. x_0, h, Γ and b represent the peak center, peak height, FWHM and background, respectively.

A number of grains with orientations other than [001]//LD were also examined, particularly for [110]//LD and [111]//LD grains. However, no obvious band structure was found in these grains, in contrast with the distinct band network measured in [001] grains. For example, **Fig. S3a** and b shows the $(6\bar{6}0)$ lattice strain map in ND and the diffraction peak FWHM map for a fatigued [110]//LD grain, respectively. No band structure could be identified from these maps.

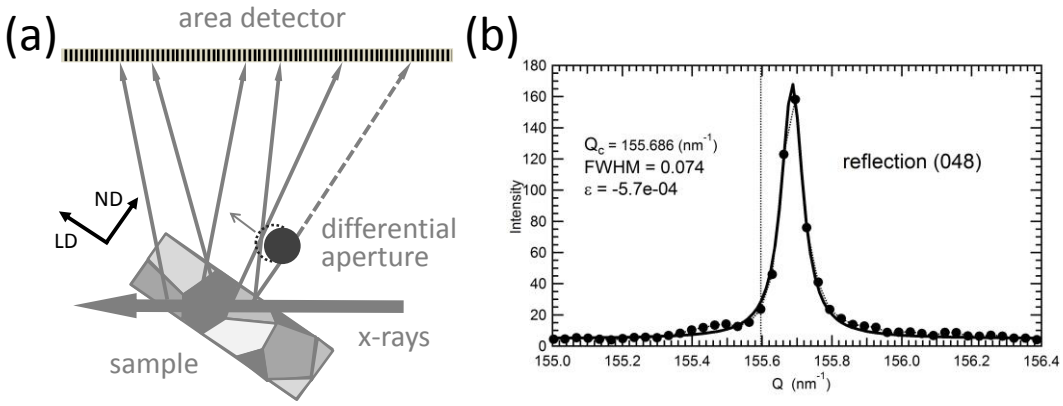

Fig. S2. Setup of synchrotron based μXRD measurement. **(a)** Schematic illustration of the diffraction geometry. **(b)** Diffraction line profile of |**q**|-distribution.

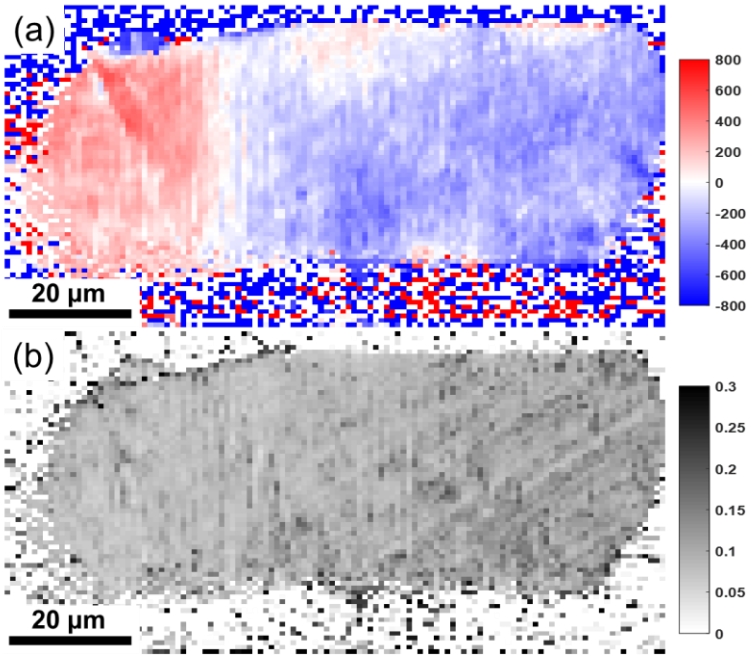

Fig. S3. μXRD maps in a fatigued [110]//LD grain. **(a)** A two-dimensional map of $(6\bar{6}0)$ lattice strain in ND. **(b)** A map of the $(6\bar{6}0)$ diffraction peak FWHM.

S4. Determination of slip planes of the observed slip bands

Three Euler angles (1) (φ_1, Φ, φ_2) of the measured grain with respect to the global coordinate system x-y-z (fixed within the laboratory frame as shown in **Fig. S4a**) is determined directly from μXRD measurements. A vector **h** can be represented as the Miller indices (2) $[h^0_1, h^0_2, h^0_3]$ in the crystal frame that can also be represented as $[h_1, h_2, h_3]$ in

the frame of x-y-z. The transformation of the indices between the two coordinate systems is given by

$$\begin{bmatrix} h_1^0 \\ h_2^0 \\ h_3^0 \end{bmatrix} = \begin{bmatrix} \cos\varphi_1\cos\varphi_2 - \sin\varphi_1\sin\varphi_2\cos\Phi & \sin\varphi_1\cos\varphi_2 + \cos\varphi_1\sin\varphi_2\cos\Phi & \sin\varphi_2\sin\Phi \\ -\cos\varphi_1\sin\varphi_2 - \sin\varphi_1\cos\varphi_2\cos\Phi & -\sin\varphi_1\sin\varphi_2 + \cos\varphi_1\cos\varphi_2\cos\Phi & \cos\varphi_2\sin\Phi \\ \sin\varphi_1\sin\Phi & -\cos\varphi_1\sin\Phi & \cos\Phi \end{bmatrix} \begin{bmatrix} h_1 \\ h_2 \\ h_3 \end{bmatrix} \quad (1)$$

The third coordinate x ′-y ′-z ′associated with the incident X-ray beam is also introduced, as shown in **Fig. S4a**. The coordinate of **h** in this frame is [h ′1, h ′2, h ′3], which can be determined by

$$\begin{bmatrix} h_1 \\ h_2 \\ h_3 \end{bmatrix} = \begin{bmatrix} 1 & 0 & 0 \\ 0 & \cos 135^\circ & \cos 45^\circ \\ 0 & \cos 135^\circ & \cos 135^\circ \end{bmatrix} \begin{bmatrix} h_1' \\ h_2' \\ h_3' \end{bmatrix} \quad (2)$$

In the x-y-z coordinate system, the algebraic equation for a plane with a normal vector **h** can be represented as

$$h_1 x + h_2 y + h_3 z = c \quad (3)$$

Different values of *c* in Eq. (3) correspond to different planes with the same normal vector **h**, but all of them are parallel to each other. Likewise, the algebraic equation of a plane with normal **h** in x ′-y ′-z ′system can be obtained using the corresponding $[h_1' \ h_1' \ h_1']$. Using the above transformation relations, we calculated the orientations of the intersection lines of four {111} slip planes in x-z and x ′-y ′planes for a [001] grain, as listed in **Table S2**. Note that the x-y plane is the slicing plane mapped by μXRD and the x ′-y ′ plane corresponds to the sample surface plane. Also note that the two slip planes of (111) and $(1\bar{1}1)$ almost coincide with the x-y plane, but largely deviate from the x ′-y ′plane. On the surface of the [001] grain, we used optical microscopy to observe three sets of slip traces, i.e., intersection lines of {111} slip planes (not shown here). From the above analysis of intersection lines, we can associate these three sets of slip traces with the intersection lines from (111), $(11\bar{1})$ and $(1\bar{1}1)$ slip planes. Likewise, the shear band network structure from

the μXRD mapping (**Fig. S4b**) can be also associated with three sets of intersection lines from the (111), ($11\bar{1}$) and ($\bar{1}11$) slip planes.

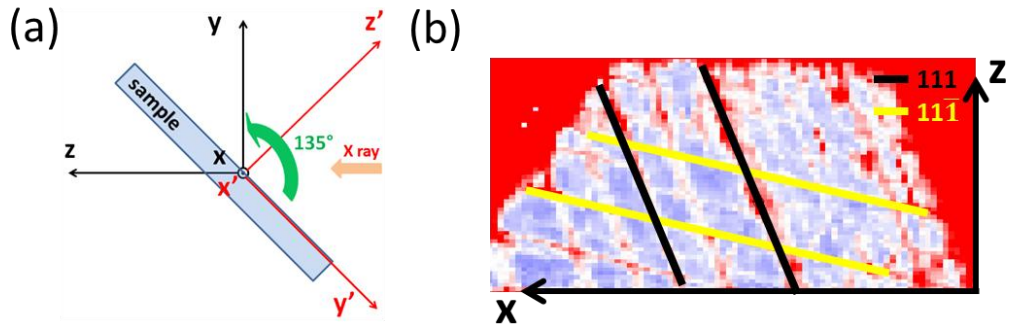

Fig. S4. Setup of μXRD measurement and analysis of {111} slip planes in multiple slip bands in a [001] grain. **(a)** Coordinate systems used for μXRD measurements. The incident X-ray is along the z axis. The surface normal direction (ND) of the sample is along the y ´ axis and the loading direction (LD) along the y ´ axis. **(b)** The shear bands in a two-dimensional μXRD map are associated with the (111) [overlapping with ($1\bar{1}1$)] and ($11\bar{1}$) slip planes, marked with black and yellow lines, respectively.

Table S2. Calculated orientations of slip lines (from different {111} slip planes) **in x-z and x ´-z ´planes**

Slip plane	Angle to x axis in x-z plane	Angle to x ´axis in x ´-z ´plane
($11\bar{1}$)	13.1 °	15.7 °
(111)	69.3 °	107.8 °
($\bar{1}11$)	124.9 °	109 °
($1\bar{1}1$)	68.2 °	21.3 °

S5. Evolution of diffraction profiles near the intersection of slip bands

The diffraction profiles along ND were collected with the energy scanning in the x-z plane (see **Fig. S4a**) for the fatigued specimen prior to and upon loading. **Fig. S5** shows the diffraction profiles near the intersection of M1 and M2 bands, mainly within the boxed area in **Fig. S5a**. The 'N'-shaped transition in the center position of diffraction peaks across the wall of M1 band can be reasonably associated with the pile-up edge dislocations of the

same sign. The spatial evolution of diffraction profiles indicates the dynamic dislocation activities. A decrease in strain gradient implies that some dislocations moved out of the viewing area. Lattice strains across the M1 band in the fatigued specimen before loading is displayed in **Fig. S6**. Importantly, the lattice strain at the wall area is given by a red bar connecting two values (i.e., two red dots), which correspond to two spilt diffraction peaks at one measurement pixel. Evidently, the lattice strain distribution is asymmetrical at the intersection between the M1 and M2 bands.

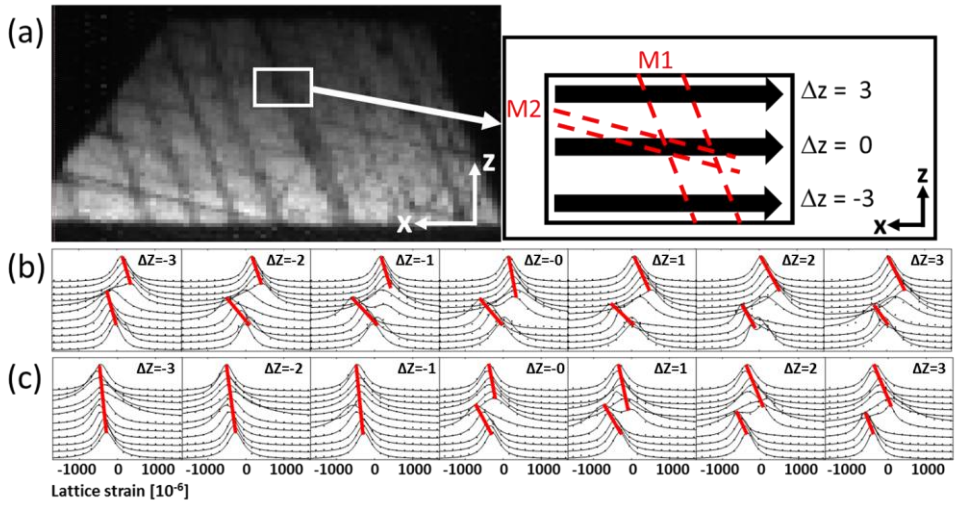

Fig. S5. Evolution of diffraction profiles near the intersection of M1 and M2 bands, suggesting the dynamic changes of dislocation configurations. **(a)** A map of the (480) diffraction peak FWHM, $\mathbf{q}_{\mathrm{FWHM}}$, in a [001] grain and a schematic showing the measurements of diffraction profiles at different positions in the x-z plane. **(b)** Peak profiles in the boxed area indicated in **(a)** before further tensile loading; curves in each panel correspond to peak profiles at the same Δz, but different x (from left to right). **(c)** Same as **(b)**, except after applying a tensile load.

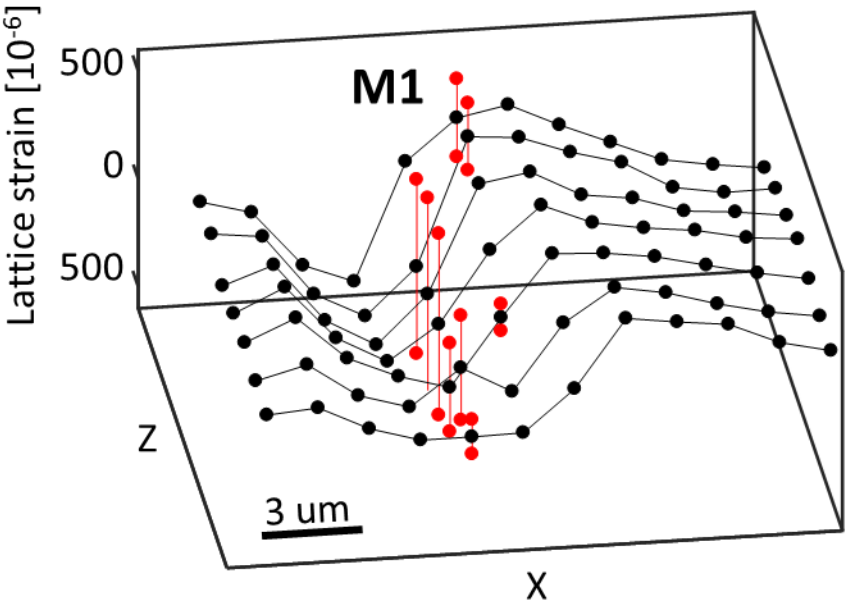

Fig. S6. Elastic strain distributions near the intersection of M1 and M2 bands.

S6. Analysis of elastic strain field near intersection of dislocation pile-ups

The method for determining the stress field and lattice strain distribution at the intersection of edge dislocation pile-ups is described in this section. Two arrays of edge dislocation pile-ups with same sign are constructed, as shown in **Fig. S7** by the thick red dashed line and the thin red dashed line, respectively. In the crystal frame, the horizontal loading direction is along [100] and the diffraction vector is along [012]. The slip plane of the broad slip band is (111) with the Burgers vector along $[10\bar{1}]$ and that of the thin slip band is $(11\bar{1})$ with the Burgers vector along [011]. Thus, the primary and secondary slip systems are $[10\bar{1}]$ (111) and [011] $(11\bar{1})$, respectively. The length of dislocation arrays of the broad slip band is denoted as I and the length of dislocation arrays in the thin slip band is M. According to TEM observations, the spacing of two neighboring dislocations with the same sign in the secondary slip system is about 100 nm. The spacing of two neighboring dislocations along the dislocation array in the broad band is represented by a variable L, varying between 20~200 nm. A cubic volume element with a size of $1000 \times 1000 \times 1000$ nm^3 is estimated as the effective diffraction voxel for determining the lattice strain distribution.

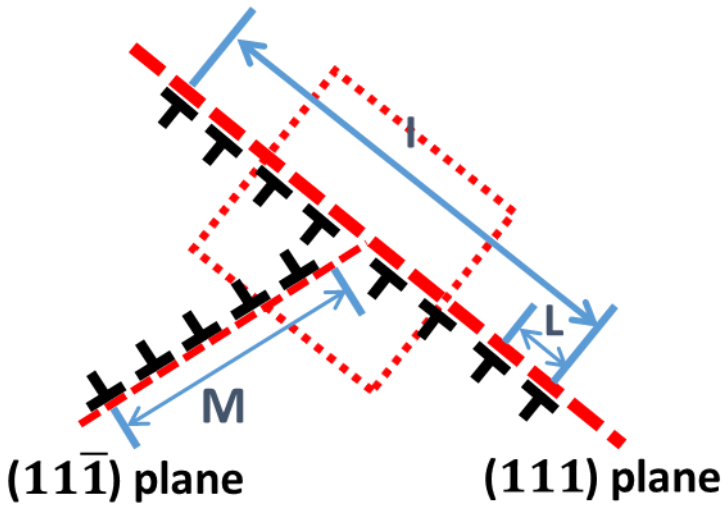

Fig. S7. Schematic diagram showing the geometry of dislocation arrays in the primary and secondary slip bands. The horizontal loading direction (LD) is close to [100]. The diffraction vector direction is [012]. The primary slip system is $[10\bar{1}](111)$ and the secondary slip system is $[011](11\bar{1})$.

To a first approximation, we determine the elastic stress field generated by dislocation arrays within an isotropic medium. The resultant stress distribution induced by the above-mentioned dislocation configurations is evaluated by summing up the stress field of individual dislocations according to (3)

$$\sigma_{xx} = -\frac{Gb}{2\pi(1-\nu)}\frac{y(3x^2+y^2)}{(x^2+y^2)^2} \tag{4}$$

$$\sigma_{xy} = \frac{Gb}{2\pi(1-\nu)}\frac{x(x^2-y^2)}{(x^2+y^2)^2} \tag{5}$$

$$\sigma_{yy} = \frac{Gb}{2\pi(1-\nu)}\frac{y(x^2-y^2)}{(x^2+y^2)^2} \tag{6}$$

$$\sigma_{zz} = -\frac{Gb\nu}{\pi(1-\nu)}\frac{y}{(x^2+y^2)^2} \tag{7}$$

$$\sigma_{xz} = 0 \tag{8}$$

$$\sigma_{yz} = 0 \tag{9}$$

where G and ν are Young's modulus and Poisson's ratio, respectively. The normal stress

σ_n along the diffraction vector is calculated by

$$\sigma_n = \sigma_{xx}l^2 + \sigma_{yy}m^2 + \sigma_{zz}n^2 + 2\sigma_{xy}lm + 2\sigma_{yz}mn + 2\sigma_{zx}nl \quad (10)$$

where *l*, *m* and *n* represent the direction cosines of the diffraction vector in the dislocation coordinate system. The elastic strains at the location of 500 nm upper and below the dislocation plane can be calculated from the stress field described above. Thus, the lattice strain along the diffraction vector as a function of *L* is plotted in the inset of **Fig. 4b**. From the measured strain difference of the split diffraction peaks (about 840 με along ND, i.e., diffraction vector direction) near the intersection of M1 and M2 bands, we estimated the average spacing, *L*, of the edge dislocation array in the M1 band as about 100 nm and the length of dislocation arrays *I* and *M* as ~10 μm. Thus there are about 100 edge dislocations with the same sign accumulated in the left portion of the wall of M1 band (near its intersection with M2 band).

S7. Dislocation dynamics simulations

A two-dimensional dislocation dynamics model was used to simulate the equilibrium dislocation configuration near the intersection of slip bands, as measured from μXRD experiments. The active slip systems associated with the primary and secondary slip bands are shown in **Fig. S7**. The fixed boundary conditions are used to relax the system. Besides the dislocation pile-up arrays in the primary and secondary slip systems, an equal number of positive and negative dislocations are randomly distributed in the primary slip band. The dislocation density within the primary shear band and matrix is 4×10^{14} m^{-2} and 1×10^{14} m^{-2}, respectively. The annihilation of dislocations is neglected. The applied shear stress in the simulation cell, elastic modulus, and Poisson's ratio are taken as 100 MPa, 190 GPa, and 0.3, respectively.

References

1. Bunge HJ, Texture analysis in materials science: Mathematical methods. 1982, London: Butterworth.

2. Ashcroft NW and Mermin ND, Solid state physics, ISBN# 0-03-083993-9 (college edition) 1976.
3. Mittemeijer EJ, Welzel U (2008) The “state of the art” of the diffraction analysis of crystallite size and lattice strain. Zeitschrift für Kristallographie (International journal for structural, physical, and chemical aspects of crystalline materials) 223: 552–560.